

## Highly selective standoff detection and imaging of trace chemicals in a complex background using single-beam coherent anti-Stokes Raman scattering

Marshall T. Bremer, Paul J. Wrzesinski, Nathan Butcher, Vadim V. Lozovoy, and Marcos Dantus<sup>a)</sup>

*Department of Chemistry, Michigan State University, East Lansing, Michigan 48824, USA*

(Received 28 March 2011; accepted 22 August 2011; published online 9 September 2011)

A non-destructive and highly selective method of standoff detection is presented and quantitatively evaluated. The method is found to be orders of magnitude more sensitive than previous coherent spectroscopy methods, identifying concentrations as low as  $2 \mu\text{g}/\text{cm}^2$  of an explosive simulant mixed in a polymer matrix. The approach uses a single amplified femtosecond laser to generate high-resolution multiplex coherent anti-Stokes Raman scattering (CARS) spectra encompassing the fingerprint region ( $400\text{--}2500 \text{ cm}^{-1}$ ) at standoff distance. Additionally, a standoff imaging modality is introduced, visually demonstrating similar sensitivity and high selectivity, providing promising results toward highly selective trace detection of explosives or warfare agents. © 2011 American Institute of Physics. [doi:10.1063/1.3636436]

The desire to detect hazardous chemicals at standoff distances has led to the research and development of many laser based techniques with the hopes of immediate application to the areas of defense, national security, and environmental disasters.<sup>1–3</sup> In particular, the low vapor pressure of common explosives has stimulated research in detecting trace quantities in the condensed phase.<sup>2,3</sup> Non-destructive techniques based on fluorescence, infrared (IR) absorption, or THz absorption spectroscopies can detect trace quantities; however, they have yet to be shown effective in the presence of a complex, condensed-phase chemical background. The unique chemical “fingerprint” and sharp spectral features provided by Raman scattering give this spectroscopy an advantage for positive chemical identification within a complex environment.<sup>4</sup> However, benchmarks in Raman based detection in a standoff configuration have been limited to macroscopic quantities due to the low Raman scattering cross section,<sup>5</sup> and efforts toward detecting trace quantities have yet to compete with the sub  $\mu\text{g}/\text{cm}^2$  sensitivity demonstrated by the absorption based methods.<sup>6–10</sup> The method detailed here provides  $\mu\text{g}/\text{cm}^2$  sensitivity with Raman specificity using less than  $8 \mu\text{J}$  laser pulses in the near IR.

Coherent anti-Stokes Raman scattering (CARS) spectroscopy achieves the same chemical specificity as Raman spectroscopy with greatly enhanced signal and no single-photon fluorescence interference, leading several groups to pursue this as a standoff or arms-length detection technique<sup>11–14</sup> and quantitatively compare this coherent method to spontaneous Raman.<sup>14</sup> The traditional two-color CARS scheme, often used for microscopy, requires spatial and temporal overlap of two beams and wavelength tuning of one laser to generate the full spectrum offered by Raman spectroscopy. In contrast, single-beam CARS uses a single femtosecond laser to yield an entire spectrum in a single laser shot. This provides a more convenient experimental

setup for standoff detection applications. This technique, originally developed for microscopy,<sup>15</sup> was demonstrated for standoff detection in 2008<sup>12</sup> and subsequently demonstrated on real explosives.<sup>13</sup> These reports show the ability of this approach to acquire CARS spectra from bulk and mixed samples as well as small crystals at standoff distances up to 12 m (limited by lab space) with and without a reflecting substrate.

Despite the promised benefits of CARS for standoff detection, there has yet to be reported detection limits on par with laser absorption based methods or a demonstration of the specificity within a complex chemical environment. Here, we achieve detection limits competitive with less chemically specific non-destructive methods<sup>8–10</sup> and simultaneously demonstrate impressive selectivity with standoff chemical images.

In the single-beam CARS measurements performed here, an ultrashort pulse induces a vibrational coherence in the ground state molecular ensemble of all vibrational states overlapped by the bandwidth of the laser. The probe photons, with a much narrower bandwidth and perpendicular polarization, scatter off this coherence producing a fourth beam which is blue-shifted from the probe by the frequency of the resonance.

A schematic of the experimental setup is shown in Figure 1(a). An amplified fs-laser focused in an argon-filled waveguide (AFWG) generates an ultra broadband continuum capable of exciting vibrations in the range  $0\text{--}3000 \text{ cm}^{-1}$ . The amplified laser and AFWG are described elsewhere;<sup>16</sup> however, we have elected to use pure argon at 5 psi above atmosphere in the AFWG. The pulse shaper compresses and shapes the continuum (phase, polarization and amplitude) to deliver the desired pulse at the target. Multiphoton intrapulse interference phase scan (MIIPS) is used to measure and correct phase distortions.<sup>17</sup> A simple telescope was used to provide a  $\sim 100 \mu\text{m}$   $1/e^2$  focal diameter at 1 m, and in all experiments, the pulse energy is reduced to less than  $8 \mu\text{J}/\text{pulse}$  ( $8 \text{ mW}$  average power) to avoid sample damage. For simplicity, CARS emission was collected by a separate small diameter (30 mm) lens, allowed by the specular nature of the target. Emission with

<sup>a)</sup> Author to whom correspondence should be addressed. Electronic mail: dantus@msu.edu.

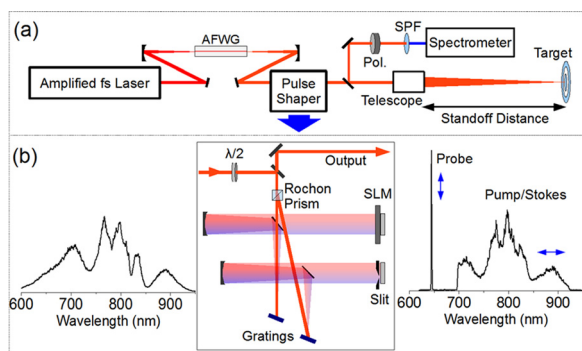


FIG. 1. (Color online) Schematic of the single-beam CARS setup (a) and modified pulse shaper with typical before and after spectra (b). Pol.: Polarizer; SPF: short pass filter; blue double arrows indicate polarization of spectral components. Delay stage in probe arm of shaper is not shown.

polarization perpendicular to probe pulse is absorbed by the polarizer, and laser emission is suppressed by a short pass filter. The resulting CARS signal is recorded with a 27 cm spectrometer and a back illuminated CCD (Princeton Instrument's PIXIS100) and presented in wavenumber units with respect to the probe.

The non-resonant background, traditionally a significant drawback of CARS compared to spontaneous Raman, is reduced due to the small temporal overlap of the ultrashort pump/Stokes portion with the narrowband probe. A polarization based probe discrimination scheme, introduced elsewhere,<sup>18</sup> and spectral separation of the probe from the pump/Stokes are used to eliminate the resonant and non-resonant contributions due solely to the pump/Stokes portion of the pulse (Fig. 1(b)). These background suppression techniques are implemented within the pulse shaper.

It is appropriate to describe the pulse shaper (Fig. 1(b)) in detail due to several modifications which are responsible for improvements in resolution, background suppression, and signal intensity. While a traditional dual mask spatial light modulator (SLM) pulse shaper is capable of polarization or amplitude shaping in addition to phase shaping, here we have effectively created a double pulse shaper, one shaper for each polarization component. A waveplate rotates the polarization of the laser, and the Rochon prism passes the horizontal component (for the pump/stokes) to the traditional SLM based shaper. The vertical component (probe) is directed to a simple folded 4-f shaper which selects a narrowband feature with a slit at the Fourier plane. The two components are recombined within the Rochon prism. The waveplate controls the distribution of energy between the probe and the pump/Stokes arms, typically at a ratio of about 9:1.

There are three benefits of this setup. First, the Rochon prism offers a high contrast ratio ( $>10^4$ ) and accordingly good polarization based background suppression. Second, a tradeoff between excitation bandwidth and probe resolution occurs with the 640 pixel SLM which is avoided by the use of a slit at the Fourier plane in the probe arm. Finally, amplitude shaping is possible in this scheme, allowing reduction of the ultra-short ( $\sim 7$  fs) excitation pulse energy below the damage threshold while retaining the maximum intensity in the harmless probe pulse (picoseconds).

Detection of trace compounds is most challenging when the analyte of interest is dissolved in a complex matrix. For

this study, samples are thin films consisting of small quantities of dinitrotoluene (DNT) dissolved in a polymer solution and spin coated on gold-coated silicon wafers (Platypus Technologies). Polymer solutions are polystyrene (PS) or polymethylmethacrylate (PMMA) dissolved in toluene.

CARS spectra obtained from PS and PMMA films containing various concentrations of 2,4DNT at 1 m standoff and with 1 s of collection are shown in Fig. 2. The CARS lines from PS, PMMA, residual toluene, and air form a complex background in which the  $1350\text{ cm}^{-1}$  DNT feature is still visible at 2% concentration. The DNT concentration in the 2% samples is  $\sim 200\text{ mg/cm}^3$  or  $10\text{ }\mu\text{g/cm}^2$  in the  $5\text{ }\mu\text{m}$  thick PS film (Fig. 2(a)) and  $<5\text{ }\mu\text{g/cm}^2$  in the  $2.1\text{ }\mu\text{m}$  PMMA film (Fig. 2(b)). Additional features of air and signal from  $2\text{ }\mu\text{g/cm}^2$  of DNT are observed in Fig. 2(c).

An imaging modality was introduced as a further demonstration of the sensitivity and selectivity of this technique. By recording the difference in intensity at and adjacent to a particular resonance in the spectrally resolved signal and raster scanning the sample, intensity maps of several resonances were created simultaneously and displayed in Figure 3. These images were obtained at 1 m standoff with 0.5 s of accumulation per pixel (500 laser pulses). Note that there is no background subtraction or processing of the acquired spectra while making these images.

The imaged area in Figure 3(a) contains PS, PMMA, toluene, and DNT on distinct substrates with varying thickness and sample structure. Panel 3(a)-PMMA shows PMMA

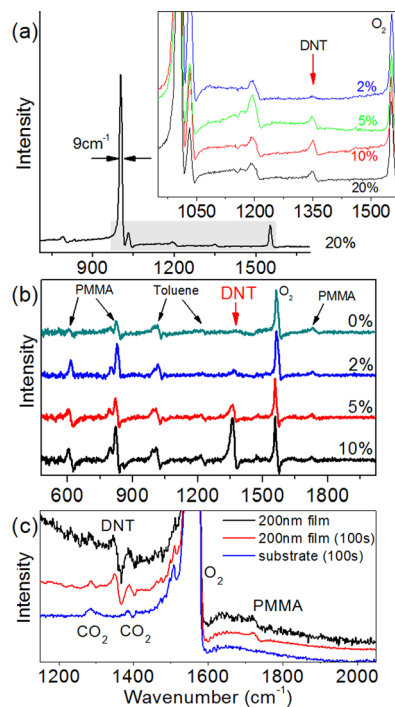


FIG. 2. (Color online) CARS spectra acquired at 1 m standoff on  $<5\text{ }\mu\text{m}$  PS films (a),  $<2.5\text{ }\mu\text{m}$  PMMA films (b), and 200 nm PMMA film containing 10% DNT (c). Percentages refer to the concentration of 2,4DNT in the film relative to polymer mass. Unprocessed (a) and processed spectra (b) show detection of the  $1350\text{ cm}^{-1}$  DNT feature at 2% concentration. Unprocessed spectra in (c) shows signal from a blank substrate (bottom spectrum) and 200 nm film (middle) integrated for 100 s to clarify features in the low signal to noise 1 s exposure (top).  $\text{CO}_2$  and the ro-vibrational features of  $\text{O}_2$  are also visible in (c).

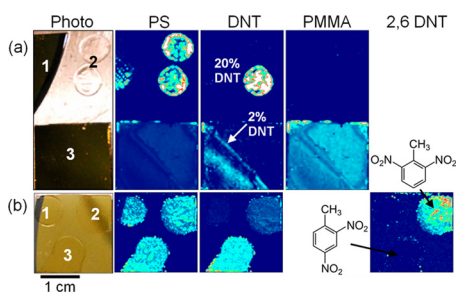


FIG. 3. (Color online) Stand-off chemical images created at 1 m. Title on each chemical image refers to the resonance monitored: PS =  $1200\text{ cm}^{-1}$ , DNT =  $1350\text{ cm}^{-1}$ , PMMA =  $1750\text{ cm}^{-1}$ , and 2,6-DNT =  $1090\text{ cm}^{-1}$ . Three types of samples in (a) show trace detection in a complex environment, 1: PS fingerprint on wafer; 2: two drops of PS on aluminum substrate  $\sim 100\text{ }\mu\text{m}$  thick; 3:  $3\text{ }\mu\text{m}$  PMMA film with half containing DNT. Residual toluene makes the PMMA film visible in the PS panel. The final panel reveals trace amount of DNT (one PS drop at 20% and half of the PMMA film at 2%). Three  $\sim 3\text{ }\mu\text{m}$  films in (b) show isomer discrimination, 1: pure PS; 2: 2,6-DNT in PS at 20%; and 3: 2,4-DNT in PS at 20% concentration. Images were individually normalized and some are displayed saturated to emphasize small signals. Image dimensions: (a)  $50 \times 100$  pixels and (b)  $50 \times 50$  pixels.

detection in the  $3\text{ }\mu\text{m}$  film with no false positive from the PS in fingerprint form or drop coated on aluminum. In panel 3(a)-DNT, DNT is observed in only one PS drop and half of the PMMA film. We see high contrast in the PMMA film with only 2% DNT concentration, demonstrating chemical imaging at  $<10\text{ }\mu\text{g}/\text{cm}^2$ .

Figure 3(b) attests to the specificity of the method by showing discrimination between isomers of DNT. Figure 3(b)-DNT maps the intensity of the  $1350\text{ cm}^{-1}$  resonance shared by both isomers, while 3(b)-2,6DNT monitors the  $1090\text{ cm}^{-1}$  resonance unique to 2,6 DNT.

Intensity maps created using selective excitation are displayed in Figure 4. The pulse shaper creates a pair of chirped pulses to selectively excite a particular resonance as described by Wrzesinski *et al.*,<sup>19</sup> and the spectrally integrated signal intensity is recorded. Although a spectrometer was used, this technique allows use of a single detector with associated potential for high speed imaging.

The chemical images presented effectively demonstrate the sensitivity and selectivity of this standoff detection technique. Beyond this purpose, they support the potential of CARS to extend Raman chemical imaging for forensic applications into the standoff domain with similar sensitivity,<sup>4</sup> allowing interrogation of surfaces which are impractical using traditional microscopy methods.

The present limit of detection (LOD) for this technique is  $<2\text{ }\mu\text{g}/\text{cm}^2$ , when using 8 mW of average laser power focused to a  $100\text{ }\mu\text{m}$  diameter and averaging for 1 second. This LOD is achieved on the minority constituent of a hydrocarbon mixture. In other words, this method can determine if an amount equal or greater than  $10^{-10}\text{ g}$  of explosive material is present at the focal spot, with little regard for the material on which it is deposited or with which it is mixed. This

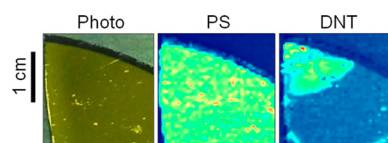


FIG. 4. (Color online) Standoff chemical images created at 1 m using selective excitation. The two intensity maps were created with 2 separate scans with 0.5 s of accumulation per pixel. The title refers to the selectively excited resonance: PS =  $1200\text{ cm}^{-1}$  and DNT =  $1350\text{ cm}^{-1}$ . Only the corner of the  $5\text{ }\mu\text{m}$  film contains DNT (40% concentration). Image dimensions:  $40 \times 40$  pixels.

shows great promise for non-destructive imaging and sensing of hazardous materials in the real world. Our project is still in the exploratory phase and a number of parameters can be readily improved upon through the choice of laser source, detection optics, and electronics. These efforts are presently underway.

Funding for this research was provided by the Department of Homeland Security, Science and Technology Directorate, under Contract No. HSHQDC-09-C-00135 (Dr. Michael Shepard, Program manager), administered by The Johns Hopkins University, Applied Physics Laboratory (Dr. Jane M. Spicer and Dr. Joseph A. Miragliotta, Program Managers).

<sup>1</sup>D. S. Moore, *Rev. Sci. Instrum.* **75**, 2499 (2004).

<sup>2</sup>S. Wallin, A. Pettersson, H. Östmark, and A. Hobro, *Anal. Bioanal. Chem.* **395**, 259 (2009).

<sup>3</sup>U. Willer and W. Schade, *Anal. Bioanal. Chem.* **395**, 275 (2009).

<sup>4</sup>A. Tripathi, E. Emmons, P. Wilcox, J. Guicheteau, D. Emge, S. Christensen, and A. Fountain, *Appl. Spectrosc.* **65**, 611 (2011).

<sup>5</sup>J. C. Carter, S. M. Angel, M. Lawrence-Snyder, J. Scaffidi, R. E. Whipple, and J. G. Reynolds, *Appl. Spectrosc.* **59**, 769 (2005).

<sup>6</sup>M. Gaft and L. Nagi, *Opt. Mater.* **30**, 1739 (2008).

<sup>7</sup>B. Zachhuber, G. Ramer, A. Hobro, E. Chrysostom, and B. Lendl, *Anal. Bioanal. Chem.* **400**, 2439 (2011).

<sup>8</sup>L. C. Pacheco-Londoño, W. Ortiz-Rivera, O. M. Primera-Pedrozo, and S. P. Hernández-Rivera, *Anal. Bioanal. Chem.* **395**, 323 (2009).

<sup>9</sup>R. Furstenberg, C. A. Kendziora, J. Stepnowski, S. V. Stepnowski, M. Rake, M. R. Papantonakis, V. Nguyen, G. K. Hubler, and R. A. McGill, *Appl. Phys. Lett.* **93**, 224103 (2008).

<sup>10</sup>C. W. Van Neste, L. R. Senesac, and T. Thundat, *Anal. Chem.* **81**, 1952 (2009).

<sup>11</sup>C. H. R. Ooi, G. Beadie, G. W. Kattawar, J. F. Reintjes, Y. Rostovtsev, M. S. Zubairy, and M. O. Scully, *Phys. Rev. A* **72**, 023807 (2005).

<sup>12</sup>H. Li, D. Harris, B. Xu, P. Wrzesinski, V. Lozovoy, and M. Dantus, *Opt. Express* **16**, 5499 (2008).

<sup>13</sup>O. Katz, A. Natan, Y. Silberberg, and S. Rosenwaks, *Appl. Phys. Lett.* **92**, 171116 (2008).

<sup>14</sup>A. Portnov, S. Rosenwaks, and I. Bar, *Appl. Phys. Lett.* **93**, 041115 (2008).

<sup>15</sup>N. Dudovich, D. Oron, and Y. Silberberg, *Nature* **418**, 512 (2002).

<sup>16</sup>H. Li, D. A. Harris, B. Xu, P. J. Wrzesinski, V. V. Lozovoy, and M. Dantus, *Appl. Opt.* **48**, B17 (2009).

<sup>17</sup>Y. Coello, V. V. Lozovoy, T. C. Gunaratne, B. Xu, I. Borukhovich, C.-hung Tseng, T. Weinacht, and M. Dantus, *J. Opt. Soc. Am. B* **25**, A140 (2008).

<sup>18</sup>D. Oron, N. Dudovich, and Y. Silberberg, *Phys. Rev. Lett.* **90**, 213902 (2003).

<sup>19</sup>P. Wrzesinski, D. Pestov, V. V. Lozovoy, and M. Dantus, (unpublished).